Available online at www.sciencedirect.com
ScienceDirect
Geochimica et Cosmochimica Acta 70 (2006) 5617–5633
Geochimica
www.elsevier.com/locate/gca

Thermodynamic studies of pyrrhotite–pyrite equilibria in the Ag–Fe–S system by solid-state galvanic cell technique at 518–723 K and total pressure of 1 atm

Evgeniy G. Osadchii *, Dmitriy A. Chareev

Institute of Experimental Mineralogy, Russian Academy of Sciences, Chernogolovka, Moscow District 142432, Russia

Received 25 August 2005; accepted in revised form 15 August 2006

Abstract

The reaction $FeS_2(cr) + 2Ag(cr) = 'FeS'(cr) + Ag_2S(cr)$ was studied by measuring the temperature dependence of the electromotive force (EMF) of the all-solid-state galvanic cell with common gas space:

$$(-)Pt|Ag|AgI|Ag_2S,'FeS', FeS_2|Pt(+)$$

The measurements were carried out in the flow of argon at atmospheric pressure to prevent oxidation. AgI was used as a solid electrolyte. From the measurements of EMF as a function of temperature, two linear ($\Delta_r C_p = 0$) trends were obtained, which characterize the equilibrium hexagonal pyrrhotite + pyrite (po + py) and the β–γ first-order phase transition in hexagonal pyrrhotite ($\Delta_{trs}H_m$ (γ–β) = (4020 ± 200) J mol^{-1}) at (601 ± 2) K. The latter is presumably related to the γ-paramagnetic-β-antiferromagnetic Neel's transition. For these measurements, the lower temperature limit (518 K) corresponds to the equilibrium sulfides + metallic silver ($E = 0$); and the upper temperature limit (723 K) is determined by the upper temperature at which the contribution of electron conductivity to AgI ion conductive properties may be significant. From experimental results of this study and literature data for Ag_2S, the temperature dependence of the gaseous sulfur activity was determined in the following equilibria: pyrite + high-temperature hexagonal pyrrhotite (γ + py), pyrite + low-temperature pyrrhotite (β + py):

$$\log aS_2(\gamma + py) = (15.64 \pm 0.035) - (15455 \pm 23) \cdot T^{-1}, (601 < T,\ K < 723)$$

$$\log aS_2(\beta + py) = (14.95 \pm 0.05) - (15040 \pm 28) \cdot T^{-1}, (518 < T,\ K < 601)$$

The temperature dependence of the FeS activity in hexagonal pyrrhotite (a^{po}_{FeS}) calculated for the pyrrhotite–pyrite equilibrium

$$a^{po}_{FeS}(\gamma) = (0.528 \pm 9.23 \times 10^{-3}) + (2.489 \times 10^{-7} \pm 1.485 \times 10^{-5}) \cdot T, (601 < T,\ K < 723)$$

indicates that the value $a^{po}_{FeS} = (0.528 \pm 0.005)$ remains almost constant in the mentioned temperature range. At temperatures below 601 ± 2 K, $a^{po}_{FeS}(\beta)$ and the Fe/S ratio in β-po decreases with decreasing temperature, which also correlates with the appearance of magnetic order. The compositional extremum (on a T–x diagram) where hexagonal pyrrhotite is in equilibrium with pyrite results in a significant and obvious geological consequence. In all the mineral assemblages that contain hexagonal pyrrhotite and pyrite and that have reached equilibrium at a temperature below (601 ± 2) K, the same pyrrhotite composition will correspond to two different temperatures. However, the minimal temperature principle is acceptable for natural parageneses; and in many cases, the pyrrhotite geothermometer can still be very useful.

* Corresponding author. Fax: +7 96 52 49687.
E-mail address: euo@iem.ac.ru (E.G. Osadchii).

0016-7037/$ - see front matter © 2006 Elsevier Inc. All rights reserved.
doi:10.1016/j.gca.2006.08.018

1. Introduction

Among binary sulfide systems, the system Fe–S is most interesting for geologists and metallurgists. Most ore deposits contain one or several forms of iron sulfide, which also are the most abundant rock-forming sulfides. In magmatic ore deposits, the iron sulfides are dominant minerals in ore groundmass. Pyrrhotite (po, $Fe_{1-x}S$) and pyrite (py, FeS_2) are the only sulfides that can be identified as rock-forming minerals. In most studies of sulfide assemblages, Fe–S was used as a marginal system. The T–x phase diagram has been summarized by Kissin and Scott (1982) and Vaughan and Craig (1997).

The thermodynamics of the hexagonal pyrrhotite–pyrite equilibrium was extensively studied in the past (Kullerud and Yoder, 1959; Arnold, 1962; Toulmin and Barton, 1964; and references cited within). The geological and practical significance of this system was discussed in detail in a review by Barton and Skinner (1967, 1979). The most complete and extensively used experimental study of this system was published by Toulmin and Barton (1964), who used the electrum tarnishing method (Barton and Toulmin, 1964) to determine the fugacity of gaseous sulfur. In addition, the study by Toulmin and Barton verified the very important analytical relationship between the angular position of the X-ray peak (10 2) and the pyrrhotite composition, which was first obtained by Arnold (1962). Analytical review of this area of study was performed by Barker and Parks (1986). Many experimental studies (Barton and Toulmin, 1966; Boorman, 1967; Scott and Barnes, 1971; Scott, 1976; Toulmin et al., 1991; Lusk et al., 1993) considered the Fe–Zn–S system, in which the Fe–S section plays a major role. The main emphasis of these studies was the determination of the position of the po + py binary solvus in the Fe–S system and the po + py + sphalerite solvus in the Fe–Zn–S system on temperature-composition diagrams (especially at temperatures below 823 K and standard pressure). The vertical position of the solvus (composition independent of temperature) or the inclined position (composition dependent on temperature) imply the possibility of using the system as a geo-barometer or geo-thermometer, respectively.

Schneeberg (1973) used an electrochemical cell (potentiometric sensor of second kind) with separate gas space to determine the activity of gaseous sulfur (a_{S2}) above the po + py buffer, but only four experimental points were obtained in the temperature range 597–711 K. Lusk and Bray (2002) used a modified Scheneeberg's cell and their own calibrations to measure a_{S2} above the po + py equilibrium in the temperature range 518–721 K.

The high-temperature galvanic cell technique (*aka* EMF technique) used in this study is the most precise and direct method to determine the free energy of reactions in situ (Kiukkola and Wagner, 1957a,b). Fully solid-state cells with common gas space have been proved to be highly efficient for measuring the volume effects of reactions at elevated inert gas pressures (Osadchii et al., 1998) and for determining the standard thermodynamic properties of silver and gold sulfides (Osadchii and Rappo, 2004). The use of more high-temperature solid electrolytes, such as yttria-stabilized zirconia with O^{2-}-ion conductivity has allowed the study of the thermodynamics of a number of geologically important equilibria in the systems pyrrhotite–magnetite (Osadchii et al., 2002) and Ni–S–O (Osadchii et al., 1990). EMF cells with separate gas space were successfully applied to determine the FeS activity in the sphalerite solid solutions in the temperature range 850–1020 K (Osadchii and Lunin, 1994).

Another significant advantage of the EMF technique is the possibility of the accurate evaluation of thermodynamic equilibrium in the course of experimentation.

2. Thermodynamic background

The phase relations in the Ag–Fe–S system (Fig. 1) were studied by Taylor (1970). No ternary compounds between 423 and 973 K have been found. At temperatures below 521 ± 8 K and the component ratio Ag:Fe:S = 1:1:2, the stable assemblage is represented by metallic silver and pyrite. At higher temperatures these phases give way to the assemblage argentite + pyrrhotite + pyrite, and then the phase relations undergo no significant changes up to 805 K. Above 805 K, a ternary eutectic occurs. All solid phases in the system are almost pure compounds. The contents of silver in iron sulfides and iron in argentite do not exceed 0.1 at.% (Taylor, 1970), and it was also confirmed that the composition of $Fe_{1-x}S$ in the Ag_2S + po + py assemblage above 521 ± 8 K is identical to the po in the binary assemblage po + py determined by Arnold (1962) and Toulmin and Barton (1964).

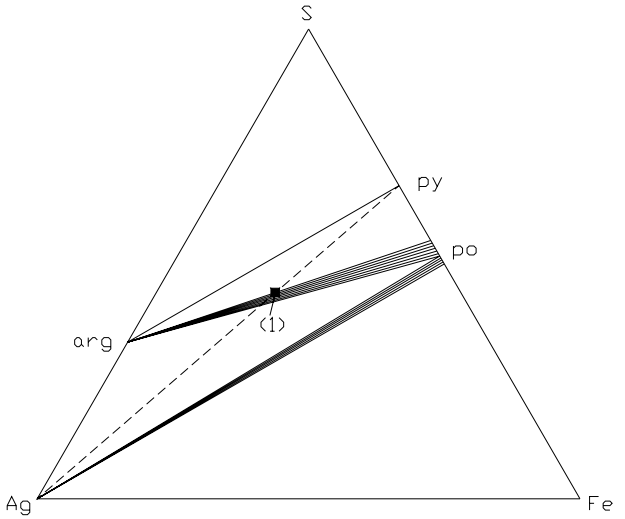

Fig. 1. Schematic representation of the phase relations in the system Ag–Fe–S in the temperature range from (518 ± 2) K to (574 ± 5) K. All known ternary compounds are not stable in the temperature range from 518 K to 723 K (source: Taylor, 1970). The diagram shows the position of Reaction (1). Abbreviation for phases: arg = Ag_2S, py = FeS_2, and po = γ or β pyrrhotite.

The phase relations are described by the solid-phase reaction:

$$FeS_2(cr) + 2Ag(cr) = \text{'FeS'}(cr) + Ag_2S(cr) \quad (1)$$

where all phases, except pyrrhotite, are in standard states (activities are equal to unity). Reaction (1) can also be presented as a sum of two reactions involving gaseous sulfur:

$$FeS_2(cr) = \text{'FeS'}(cr) + 0.5S_2(g) \quad (2)$$

and

$$2Ag(cr) + 0.5S_2(g) = Ag_2S(cr) \quad (3)$$

Under thermodynamic equilibrium conditions, the sulfur activities in Reactions (2) and (3) are equal, and in Reaction (1), the sulfur activity is eliminated.

The studied Ag–Fe–S system is considered condensed, i.e., all reactions are fully solid-phase, and the pressure of gaseous sulfur is not used as a thermodynamic parameter. The total pressure imposed on the solid phases is 1 atm Ar. Nevertheless, this approach does not exclude the possibility of presenting data in terms of gaseous sulfur activity, such as in Reactions (2) and (3). Such experimental conditions correspond to the definition of a ''condensed'' system (Kullerud and Yoder, 1959).

Reaction (1) was realized in the flow of argon in the solid-state galvanic cell with a common gas space:

$$(-)Pt|Ag|AgI|Ag_2S,\text{'FeS'}, FeS_2|Pt(+) \quad (A)$$

The vertical lines in the Cell (A) denote the phase boundaries or electric contacts with electrodes. The phases separated by commas represent the mechanical mixture of the sample system (or working electrode). The reference system (or reference electrode) is represented by pure crystalline silver. The cell polarity (shown in parentheses) on the inert platinum electrodes is dictated by the fact that the chemical potential of silver on the reference electrode is always higher than that on the working electrode. Thus, the flow of Ag^+ ions through the solid electrolyte in the cell and the flow of electrons in the external circuit are both directed from the left to the right. The EMF of the Cell (A) measured by a voltmeter is always positive, $E(A) > 0$ by definition (spontaneous process).

Cell (A) can be presented as a combination of two half-cells and Reaction (2), which serves as a sulfur source (solid-state buffer):

Left half-cell:

$$2Ag(cr) = 2Ag^+ + 2e$$

Right half-cell:

$$2Ag^+ + 2e + 0.5S_2(g) = Ag_2S(cr)$$

$$FeS_2(cr) = \text{'FeS'}(cr) + 0.5S_2(g)$$

Net potential-forming process:

$$FeS_2(cr) + 2Ag(cr) = \text{'FeS'}(cr) + Ag_2S(cr)$$

The net potential-forming process corresponds to the solid-state Reaction (1).

The EMF of the Cell (A) is related to the free energy and the equilibrium constant of Reaction (1) via the fundamental thermodynamic equation:

$$\Delta G = -nFE = -R \ln 10 T \log K \quad (4)$$

where ΔG is the Gibbs free energy change for the reaction; n is the number of electrons in the electrochemical process ($n = 2$ in Cell A); F is the Faraday constant (96484.56 J V^{-1} mol^{-1}); E is the EMF of the galvanic cell in volts; R is the gas constant (8.31441 J K^{-1} mol^{-1}); T is the absolute temperature; and K is the equilibrium constant.

If the temperature dependence $E(A) = f(T)$ is known, Eq. (4) can be used to determine the temperature dependence of the molar Gibbs energy for the Reactions (1) and (3), which are equal in equilibrium, $\Delta_r G_m(1) = \Delta_r G_m(3)$:

$$\Delta_r G_m(3) = -2FE(A) \quad (5)$$

Combining Eqs. (4) and (5) and the free energy data for the formation of argentite from silver and $S_2(g)$, one can determine a_{S2} in the Reaction (3) from $E(A) = f(T)$ measurements, as follows:

$$\log a_{S2}(3) = [\Delta_f G_m(Ag_2S, cr) + 2FE(A)]/0.5\, R \ln 10 T \quad (6)$$

Under the equilibrium conditions, $aS_2(3) = aS_2(2)$, and Eq. (6) determines the temperature dependence of the gaseous sulfur activity above the po + py couple, according to Reaction (2). In this case, the pyrrhotite compositions in equilibrium with pyrite need not be known. It is obvious that at $E(A) = 0$, the $\log aS_2(3)$ value is determined by the $Ag + Ag_2S$ equilibrium at a given temperature. Theoretically, the EMF of the Cell (A) should reach a maximum value at the line of condensation of gaseous sulfur at the standard pressure.

Eq. (6) written for a particular reaction can be used for calculating a_{S2} in all the equilibria considered in this paper. After substitution of the molar free energies of formation of Ag_2S (Richardson and Jeffes, 1952)

$$\Delta_f G_m(Ag_2S, cr) = -87.822 + 34.56 \cdot T, \text{J mol}^{-1} \quad (7)$$

And after re-arrangement, Eq. (6) becomes:

$$\log aS_2 = (-9174.5 + 20.159 \cdot E/\text{mV}) \cdot T^{-1} + 3.61 \quad (8)$$

Eq. (8) can be applied to any solid-state reactions involving the potential-forming Reaction (3).

When phases of variable composition are used, it is especially important to properly evaluate the state of equilibrium for a studied reaction. For this purpose, special kinetic experiments were performed using ''symmetrical'' cells, in which the starting compositions of the sample and reference systems only differed in pyrrhotite composition, e.g., sulfur-rich pyrrhotite and troilite (tr):

$$(+)Pt|po, py, Ag_2S|AgI|tr, py, Ag_2S|Pt(-) \quad (B)$$

In equilibrium at constant temperature and pressure, the chemical potentials of pyrrhotite (as well as a^{po}_{FeS}) on the left

and on the right electrodes are equal, assuming the same standard states. Therefore, $E(B) = 0$, since the chemical potentials of pyrite and Ag_2S are eliminated.

Under non-equilibrium conditions, a^{po}_{FeS} on the left and on the right electrodes are not equal; $a^{po}_{FeS}(l) < a^{tr}_{FeS}(r)$, since $a^{tr}_{FeS}(r) = 1$. By definition, the chemical potential of any compound is a sum of the chemical potentials of its elements. Hence, $\mu_{Fe}(l) = \mu_{Fe}(r)$, $\mu_S(l) > \mu_S(r)$, and $\mu_{Ag}(l) < \mu_{Ag}(r)$, with the latter condition causing transfer of Ag^+ ions from the right to the left. Such a situation results in EMF of the shown polarity on the inert electrodes, i.e., $E(B) > 0$. As equilibrium is attained as a result of chemical reactions on each of the electrodes, the EMF approaches zero. It is obvious that the same result would be obtained if two Cells (A) with different pyrrhotite compositions in sample systems are connected in series. This scheme can also be realized experimentally.

3. Experimental procedures

3.1. Chemicals, synthesis, and quality control

The starting chemicals were iron (Merck, 99.5%, 10 μm), silver powder (Johnson Matthey GmbH, spherical, −325 mesh, 99.9%), crystalline sulfur (Johnson Matthey, 99.9995%), and silver sulfide (Aldrich Chem. Co., 99.9%). Silver sulfide used was determined as acanthite according to X-ray analysis. All iron sulfides were obtained by dry synthesis in evacuated (10^{-4} bar) quartz glass capsules in the temperature range 673–823 K. The sealed capsules were annealed in horizontal resistance furnaces at a particular temperature (±5 K) for 5–10 days. The capsules were cooled in air.

Troilite was synthesized from pure elements, with slight excess of sulfur (about 3–5 mg per 1 g of sample), in three steps. First, iron powder and sulfur were mixed, sealed in an evacuated silica glass capsule, and annealed, with the temperature raised slowly from 473 to 673 K. After cooling, the reacted mixture was removed from the capsule, ground in an agate mortar under acetone, and placed in another quartz capsule for the second annealing at 823 K. As the third step, the mixture was ground to a homogeneous state and put in another capsule with an additional portion of fine iron powder, which was separated from the sulfide phase with a kaolin or silica wool plug (sandwich method), and annealed at 823 K for 10 days.

Pyrite was synthesized from troilite and sulfur. A slight excess of sulfur was added to the capsule, as in the pyrrhotite synthesis. Cooled capsules always contained a small amount of condensed sulfur, which was easily removable.

The equilibrium assemblage (po + py) with the molar ratio 1:1 was synthesized from troilite and sulfur in three steps with grinding in between.

All synthesized substances were examined under a microscope in reflected light and analyzed by X-ray powder diffraction (XRD, Co K_α radiation, Fe filter). The results were compared with JCPDS data. The pyrrhotite compositions were determined from the interplane distance (1 0 2), based on the $d_{(102)}$ vs. composition relationship (Toulmin and Barton, 1964). Powders of troilite and pyrite were also tested for the absence of magnetic phases.

3.2. Electrode fabrication

The sample system (working electrode) was prepared from the mixture (po + py) + Ag_2S or tr + py + Ag_2S, in which components were taken in a molar ratio of 1:1:1. The powdered mixture (400 mg) was ground for several minutes and then pressed into tablets 6 mm in diameter under the load of 1–1.2 tons. Alternatively, the same sample system was prepared from the mixture of metallic Ag powder, pyrite, and acanthite (Ag_2S), which were taken in the amounts required to provide the final product molar ratio of 1:1:1.

The reference system (reference electrode) was prepared from silver (99.9%) in the form of a cylinder 6 mm in diameter and 4 mm in thickness.

Inert platinum electrodes were cut out from a 0.5 mm foil sheet and were also made 6 mm in diameter.

The working surfaces of the electrodes were polished to a mirror luster to improve electric contacts.

3.3. Electrochemical cell design

All components of the electrochemical cell, including solid electrolyte, were sandwiched in a support tube in the order specified by the electrochemical circuit (A). The support tube was made out of a silica glass tube and had the following dimensions: ID 6.3 mm, wall thickness 1.5 mm, and length 100–150 mm (Fig. 2). Two ceramic rods were inserted into small holes in the side wall of the tube to fix the cell sandwich inside. A spring (Kanthal Super wire) was used to ensure a good physical contact between the cell components. The spring stayed in the cool zone of the cell (<500 K), and no sulfidization of the spring material was observed.

The support tube with the electrochemical cell was then placed inside a quartz glass container, in which dry argon atmosphere was maintained. The argon flow rate was 2–3 cm^3/min. Other details of the experimental design are given in Fig. 2.

3.4. Solid electrolyte and alteration of cell components

Mono-blocked AgI, synthesized and purified by the zone-melting technique at the Institute of Microelectronic Technology and Highly Pure Materials (Russian Academy of Sciences, Chernogolovka) was used as a solid electrolyte for the electrochemical cells. Plane-parallel plates 1.5–3 mm in thickness were cut out of the AgI block and then used to prepare discs with a diameter less than 6 mm. The contact surfaces of the solid electrolyte discs were also polished.

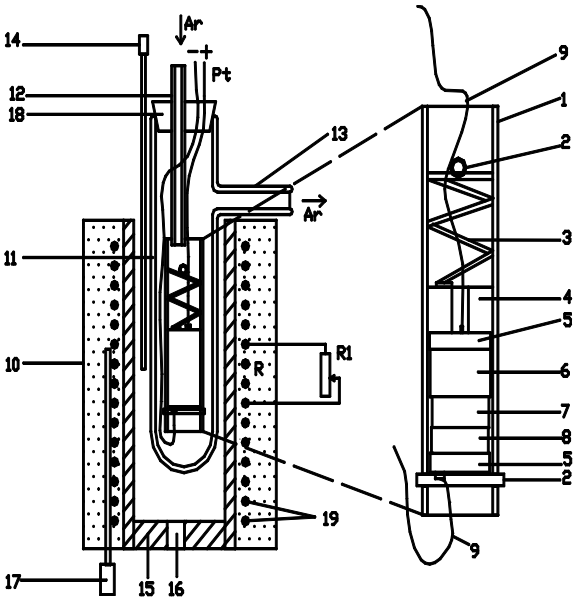

Fig. 2. Design of the electrochemical cell and resistance furnace. 1—quartz glass support tube; 2—ceramic rods inserted into the holes in the support tube; 3—spring; 4—quartz glass piston; 5—platinum electrodes; 6—sample system (right half-cell); 7—AgI solid electrolyte; 8—reference system, silver electrode (left half-cell); 9—platinum wire; 10—furnace thermal insulation layer; 11—quartz glass container; 12—inert gas inlet; 13—inert gas outlet; 14—measuring thermocouple (type K); 15—ceramic plug; 16—hole in the ceramic plug for convective air flow in the furnace; 17—regulating thermocouple; 18—rubber stopper; 19—heating coil; R—part of the heating coil connected to external rheostat R1.

No visible changes of the solid electrolyte were observed after 20–70 days of an EMF experiment. The AgI remained transparent, yellow with a slight greenish shade. Microscopic observation in transmitted and reflected light did not reveal any growth of silver or sulfide dendrites.

During the experiment all the components of the electrochemical cell adhered together, and the solid electrolyte could not be detached from either the silver electrode or the sulfide tablet without breaking. The contact of AgI with sulfides was clean, without any signs of interdiffusion. The surface of the sample system at the contact with the electrolyte was evenly altered, appearing as a tar-like "glassy" zone, which developed to a depth of 100–200 μm of the sample. During the experiment, formation of another solid phase, Ag_3SI, was also probable. Like AgI, this compound is a super-ionic conductor (Tretyakov, 1978; Ivanov-Schits and Moorin, 2000) and therefore should not affect the cell operation.

The silver reference electrode, the Pt inert electrodes, wire, and spring did not show any signs of sulfidization. Oxidation was prevented by constant argon flow through the cell. The contact of the open surfaces of the electrodes with the gas phase was limited.

3.5. Electrochemical measurements

All experiments were carried out in vertical resistance furnaces, in which inner ceramic tubes had the dimensions of 18 mm ID × 240 mm height, and the diameter of the thermal insulation wall was 160 mm (Fig. 2). To extend the length of the isothermal zone and to provide its shift towards the right direction, an external rheostat was connected in parallel to the central section of the main heating coil for a fine power tuning (Pajryd, 1985). A similar effect can be achieved by differential winding of the heater, allowing a higher density of the coil in the lower and upper parts of the furnace. The lower end of the furnace tube was closed with a ceramic stopper (with a hole 2–4 mm in diameter) to optimize the blast air flow. Via the aforesaid measures, we managed to establish a minimum 20 mm isothermal zone (±0.1 K) in the central part of the furnace. The furnaces were powered by a DC source.

Temperature in the furnace was controlled to ±0.15 K or better using a PROTERM 100 high-precision temperature controller. The regulating thermocouple (Pt/Pt, 10 mass %Rh) was placed in the immediate vicinity of the heating coil (Fig. 2).

Temperature and EMF were measured by a SCH304-2 multichannel digital millivoltmeter with accuracy of ±0.005 mV. The entrance channel resistance for EMF measurements was 10^{12}–10^{13} Ω. The cell temperature was measured by a chromel–alumel thermocouple ("K"-type).

3.6. Cell operation

For the EMF experiments, we employed the method of "temperature titration", i.e., stepwise heating and waiting for a constant (equilibrium) EMF value at each given temperature. The following procedure was used to control the accuracy and reproducibility of the EMF data. Initially, the cell was slowly heated to a certain temperature, e.g., 623 K. After the equilibrium EMF was attained, the temperature was increased in 20 K steps to the maximum value and then decreased by 10 K and further down in 20 K steps to the minimum temperature. Then, temperature was increased again by 10 K and raised in 20 K steps back to 623 K. The second temperature titration loop started at 5 K higher (628 K) and the heating continued in 10 K steps. As a result, all data points taken were 5 K apart, and the adjacent points were separated one from another by a significant period of time. For additional precision control, EMF was measured repeatedly at some points (in 5 K, 10 K, or 20 K steps).

The control time of reaching the equilibrium EMF value at a given temperature ranged from several days to 12 h. The EMF data acquisition was performed automatically in a non-stop regime with a frequency of 1 Hz, and every 5 min the three most recent measurements were averaged and saved in a computer file. These current results were plotted versus time, and the graphic visualization helped to evaluate the approach to equilibrium. The last 20–40 data points (100–200 min interval) were averaged and saved in a data table, if the EMF

values did not differ significantly from the data obtained during the previous hours. The equilibrium state was assumed when the EMF and temperature values stayed constant within ±0.02 mV and ±0.15 K, respectively, over a period of several hours to 1 day.

3.7. Control of equilibrium

Although the time to test for equilibrium was extended to as much as several days, for all experiments equilibrium was reached after no more than 48 h. After the cell was short-circuited for 10–60 s and/or polarized at 1.018 V (using a Weston cell) with direct and reverse polarity, the EMF returned to the equilibrium value within 6–24 h over the whole temperature range.

The experiments with the Cell (B) followed a special procedure. The cell was placed into a pre-heated furnace at 550, 650, or 690 K. After reaching thermal equilibrium (usually within an hour), the cell yielded EMF values from 2 to 5 mV with a clear tendency to decrease. After several hours, the EMF of the Cell (B) never exceeded 1 mV and was always positive for the above-specified polarity. After 24 h, the EMF values dropped below 0.1 mV. If temperature was raised abruptly (e.g., by 20 K over 3 min), only a few hours were necessary for the non-equilibrium EMF (no higher than 3.6 mV) to return to the equilibrium value (0 ± 0.1 mV). It should be noted that both positive and negative low-magnitude EMF values might result from an abrupt disturbance of the symmetrical cell. After the cell polarization, the equilibrium EMF values recovered within several minutes.

All of the above-described effects were clearly observed within the first day of the experiment. After two days, it was almost impossible to drive the symmetrical cell out of equilibrium.

4. Experimental results and calculations

4.1. EMF measurements

Data obtained from the EMF measurements in Cell (A) are listed in Table 1 and described by two linear ($\Delta_r C_p = 0$) equations, which refer to the fields of equilibrium of pyrite with high-temperature (γ) and low-temperature (β) pyrrhotite, respectively:

$$E(\mathrm{A})\gamma + \mathrm{py},\quad \mathrm{mV} = -(311.7 \pm 1.1) + (0.5968 \pm 0.0017)\cdot T,\quad (601 < T/\mathrm{K} < 723),\quad R^2 = 0.9999 \tag{9}$$

$$E(\mathrm{A})\beta + \mathrm{py},\quad \mathrm{mV} = -(290.9 \pm 1.4) + (0.5621 \pm 0.0025)\cdot T,\quad (518 < T/\mathrm{K} < 601),\quad R^2 = 0.9998 \tag{10}$$

The experimental errors were determined by the least-squares method for the confidence interval of 2σ.

Table 1
Measured temperatures and EMF (E_{meas}) of galvanic the Cell (A) and deviations of the experimental points from the trends calculated via Eqs. (9) and (10) ($\Delta E = E_{meas} - E_{calc}$)

T (K)	E_{meas} (mV)	ΔE (mV)
515.0[a]	0	1.39
516.5[a]	0.07	0.62
518.5[a]	0.12	−0.46
521.8[a]	2.28	−0.15
521.8[a]	2.15	−0.28
524.2	4.01	0.23
525.0	3.98	−0.25
528.0	5.85	−0.07
531.3	7.58	−0.19
531.4	7.94	0.11
532.0	7.92	−0.25
534.4	9.32	−0.19
536.3	10.55	−0.03
537.3	11.38	0.24
540.3	12.98	0.15
542.1	13.77	−0.07
546.5	16.30	−0.02
552.0	19.66	0.25
552.6	19.76	0.01
557.2	22.30	−0.03
562.6	25.31	−0.06
567.7	28.09	−0.14
568.5	28.89	0.21
572.9	31.29	0.13
573.9	31.93	0.21
578.0	34.12	0.10
578.9	34.81	0.28
582.8	36.76	0.04
583.6	37.33	0.16
584.1	37.40	−0.05
588.5	39.62	−0.31
589.4	40.27	−0.16
593.3	42.71	0.09
593.6	42.53	−0.26
594.5	43.35	0.05
598.7	45.5	−0.16
599.5	46.09	−0.02
603.8	48.89	0.26
608.8	51.61	0.00
609.8	52.26	0.05
613.5	54.97	0.55
613.8	54.75	0.15
614.8	55.00	−0.19
618.9	57.35	−0.29
620.0	58.24	−0.06
624.0	60.73	0.05
628.9	63.47	−0.14
630.1	64.24	−0.08
633.9	66.68	0.09
634.0	67.04	0.39
634.7	66.75	−0.32
638.9	69.55	−0.02
640.1	70.21	−0.08
644.1	72.77	0.09
645.2	73.14	−0.19
645.2	73.00	−0.33
649.3	75.74	−0.04
650.5	76.12	−0.38
654.4	79.07	0.25
654.5	79.07	0.19
655.8	79.59	−0.07
659.8	82.12	0.07

Table 1 (*continued*)

T (K)	E_{meas} (mV)	ΔE (mV)
661.1	82.62	−0.20
665.1	85.31	0.10
666.4	85.94	−0.05
666.5	86.36	0.31
670.3	88.32	0.01
671.5	88.85	−0.18
675.2	91.10	−0.14
675.6	91.48	0.00
676.8	92.14	−0.05
680.6	94.53	0.07
682.0	95.21	−0.09
685.6	97.40	−0.04
685.6	97.40	−0.04
687.2	98.50	0.10
687.3	98.25	−0.21
692.3	101.41	−0.03
697.6	104.66	0.05
702.8	107.67	−0.04
707.8	110.86	0.17
713.0	113.89	0.09
718.1	116.89	0.05
723.2	120.04	0.16

[a] Points excluded from calculations. See Section 5.3 for more detail explanation.

4.2. Enthalpy of β–γ phase transition

The temperature of the β–γ phase transition, $T_{trs} = (601 \pm 2)$K, was determined by simultaneously solving Eqs. (9) and (10).

The enthalpy of the first-order phase transition can be determined from the jump of the temperature derivative of the free energy or from the change of the temperature coefficient in Eqs. (9) and (10) at constant pressure. Thus, one can obtain:

$$\begin{aligned}\Delta_{trs}H_m(\gamma-\beta) &= -(\partial\Delta G(1)/\partial T)_p \cdot T_{trs} \\ &= -2F(\partial\Delta E(A)/\partial T)_p \cdot T_{trs} \\ &= (4020 \pm 200)\,\mathrm{J\,mol^{-1}} \end{aligned} \quad (11)$$

4.3. Calculation of po + py equilirbium

The temperature dependence of the gaseous sulfur activity above the pyrrhotite–pyrite equilibrium can be determined by substitution of Eqs. (9) and (10) into Eq. (8). The following Eqs. (12) and (13) were obtained by the least-squares treatment of all experimental points in Table 1 converted to $\log aS_2$ using Eq. (8):

$$\log aS_2(\gamma + \mathrm{py}) = (15.64 \pm 0.035) - (15455 \pm 23)\cdot T^{-1} \quad (12)$$

$$\log aS_2(\beta + \mathrm{py}) = (14.95 \pm 0.05) - (15040 \pm 28)\cdot T^{-1} \quad (13)$$

Fig. 3 shows the pyrrhotite–pyrite equilibrium calculated by Eqs. (12) and (13) in terms of $\log a_{S2}$ as a function of reciprocal temperature. To avoid overloading the graph, the experimental points listed in Table 1 are not shown. The temperature points from Toulmin and Barton (1964, Table 5 therein), with their location determined by Eq. (12), Schneeberg's (1973) data, and the data of this study for the β-pyrrhotite field calculated from Eq. (13) with 10-K intervals are used for comparison. The lines showing the Ag/Ag_2S and Fe/FeS(tr) equilibria were plotted from the data of Richardson and Jeffes (1952), and the S_2(g)/S(l) line was drawn from the data of Robie and Hemingway (1995).

4.4. Calculation of a^{po}_{FeS} in equilibrium with pyrite

The temperature dependence of the FeS activity in pyrrhotite in equilibrium with pyrite (po + py) can be determined using the literature data for the molar free energy of formation of troilite (Richardson and Jeffes, 1952) and pyrite (Toulmin and Barton, 1964):

$$\Delta_f G_m(\mathrm{FeS,tr}) = -150247 + 52.55\cdot T, \mathrm{J\,mol^{-1}} \quad (14)$$

and

$$\Delta_f G_m(\mathrm{FeS_2,cr}) = -298236 + 196.98\cdot T, \mathrm{J\,mol^{-1}} \quad (15)$$

In Eqs. (14) and (15), the standard state of sulfur is S_2 ideal gas at 1 bar. With the choice of literature data for FeS and FeS_2, calculated FeS activities can be directly compared to the data of Toulmin and Barton (1964) obtained for the γ-pyrrhotite field. The calculation procedure given below actually follows Eq. (18a) from Toulmin and Barton (1964) for the standard free energy of pyrite and for the evaluation of the accuracy of their experimental data.

For this calculation, the constant of the hypothetical equilibrium of pyrite, troilite, and gaseous sulfur [$\mathrm{FeS(tr)} + 0.5S_2(g) = FeS_2(cr)$, $\log K = 0.5\log aS_2(\mathrm{ref})$], which is used as a reference system with the FeS activity equal to unity, needs to be subtracted from the constant of Reaction (2) [$\log K(2) = \log a^{po}_{FeS} + 0.5\log aS_2$]. The reference equilibrium is also shown in Fig. 3. After arranging the terms, the equation for the FeS activity in pyrrhotite as a function of sulfur activity and temperature can be written as follows:

$$\log a^{po}_{FeS} = 0.5[\log aS_2(\mathrm{ref}) - \log aS_2] \quad (16)$$

The temperature (and, supposedly, enthalpy) of the β–γ transition does not depend on the pyrrhotite composition (Binary Alloy Phase Diagrams, 1987); therefore, the effect of this transition on the FeS activity in Eq. (16) should be eliminated. For this purpose, the magnitude of the γ–β transition estimated for pyrrhotite in equilibrium with pyrite (Eq. (11)) was taken into account in $\log aS_2(\mathrm{ref})$ calculations through Eq. (16).

The data from Toulmin and Barton's Table 5 (1964) accurately determine the position of the smoothed po + py equilibrium curve (no equation was given by the authors) and are completely self-consistent. For easier comparison of results, we present our data and Toulmin and Barton's (1964) data in a somewhat modified form together in Table 2.

Table 2
Data for the pyrite–pyrrhotite equilibrium from Toulmin and Barton (1964) and the present study

T/K	N_{FeS} (T & B)[a]	$(1-x)$ in $Fe_{1-x}S$[b]	$\log a(S_2)$			a_{FeS}^{po}			$\Delta_f G_m$ (FeS_2) J mol^{-1} (T & B)
			(T & B)	This study, Eq. (12)	This study, Eq. (18)	(T & B)	This study, Eqs. (16) and (12)	This study, Eqs. (16) and (18)	
1016	0.8993	0.8170	0.84	*0.424*	0.834	0.375	*0.5282*	0.330	−98,098
1009	0.9000	0.8182	0.69	*0.319*	0.698	0.374	*0.5282*	0.342	−98,814
973	0.9064	0.8288	0.00	*−0.248*	0.007	0.400	*0.5282*	0.395	−106,525
950	0.9100	0.8349	−0.43	*−0.632*	−0.438	0.414	*0.5282*	0.424	−111,248
921	0.9139	0.8414	−1.00	*−1.145*	−1.009	0.429	*0.5282*	0.454	−117,148
875	0.9200	0.8518	−1.95	*−2.027*	−1.952	0.453	*0.5282*	0.487	−126,357
872	0.9202	0.8522	−2.00	*−2.088*	−2.016	0.455	*0.5282*	0.489	−126,817
828	0.9252	0.8608	−3.00	*−3.029*	−2.989	0.477	*0.5282*	0.506	−135,608
787	0.9298	0.8688	−4.00	*−4.002*	−3.978	0.496	*0.5282*	0.516	−143,591
781	0.9300	0.8692	−4.13	*−4.153*	−4.131	0.494	*0.5282*	0.518	−144,662
750	0.9335	0.8753	−5.00	*−4.971*	−4.955	0.511	*0.5282*	0.521	−150,908
716	0.9367	0.8809	−6.00	−5.949	−5.937	0.524	0.5282	0.523	−157,582
684	0.9395	0.8859	−7.00	−6.959	−6.948	0.536	0.5282	0.524	−163,645
673	0.9400	0.8868	−7.32	−7.328	−7.318	0.537	0.5282	0.525	−165,490
654	0.9417	0.8898	−8.00	−7.995	−7.985	0.546	0.5282	0.524	−169,285
627	0.9440	0.8939	−9.00	−9.013	−9.003	0.554	0.5282	0.525	−174,364
602	0.9459	0.8974	−10.00	−10.037	−10.026	0.562	0.5282	0.524	−179,096
598	0.9462	0.8979	−10.17	−10.208	−10.198	0.564	0.5282	0.525	−179,845

Italic indicates values extrapolated into the nonlinear region (shown for comparison only).
[a] (T & B) = Toulmin and Barton (1964).
[b] $(1-x) = N_{FeS}/(2 - N_{FeS})$.

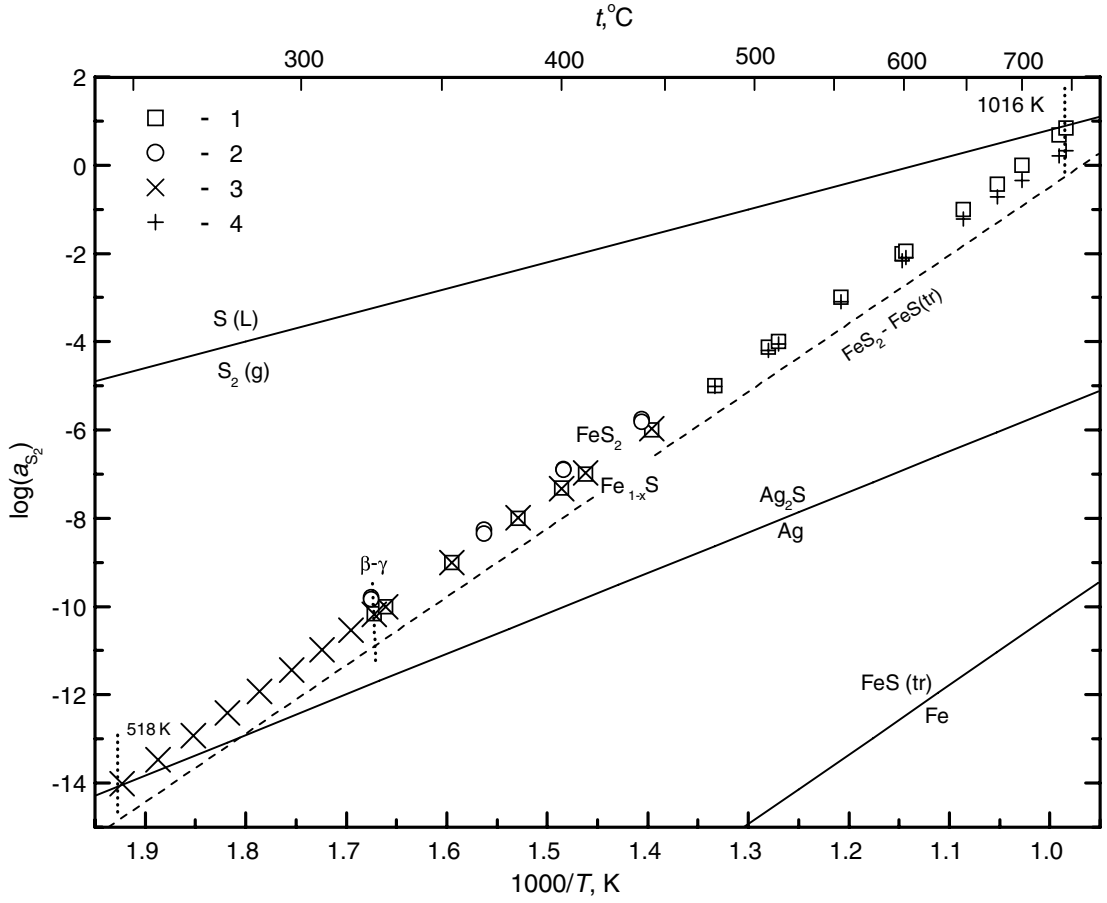

Fig. 3. Position of the pyrrhotite–pyrite equilibrium on the sulfur activity vs. temperature diagram: 1—Toulmin and Barton (1964), Table 2; 2—Schneeberg (1973); 3—This study. Calculation by Eq. (12) using the temperature points from Toulmin and Barton (1964), Table 2. In the β-pyrrhotite field, data points were calculated via Eq. (13) with 10-K intervals; 4—This study. Extrapolation by Eq. (12) into the nonlinear region using the temperature points from Toulmin and Barton (1964), Table 2. "Equilibrium" troilite–pyrite plotted using the auxiliary data Eqs. (14) and (15).

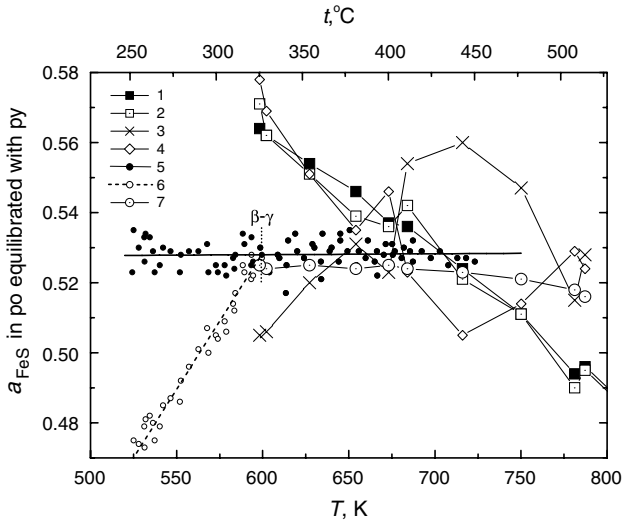

Fig. 4. Temperature dependence of the FeS activity in pyrrhotite. 1—Trend #1. Table 2, Toulmin and Barton (1964); 2—Trend #2. Recalculation of data from Table 2 (Toulmin and Barton, 1964) using Eq. (16); 3—Trend #3 (see text and Table 3 for explanation); 4—Trend #4 (see text and Table 3 for explanation); 5—Trend #5. This study (Table 3). Recalculation of experimental data from Table 1 using Eq. (16) accounting for the γ–β transition in hexagonal pyrrhotite. Line corresponds to Eq. (17); 6—Trend #6. This study. Experimental data on β + py equilibrium (Table 1) calculated without accounting for the γ–β transition in hexagonal pyrrhotite. 7—Trend #7. Calculation by Eq. (18) for the temperature dependence of $\log a_{S2}$ for the γ + py solvus over its entire stability field (Toulmin and Barton, 1964 and present study).

For calculating the values in Table 2, the data for the free energies of formation of argentite (Eq. (7)), troilite (Eq. (14)), and pyrite (Eq. (15)) from pure elements and S_2(g) were used. The data for the free energy of formation of pyrite (Eq. (15)) are secondary, since they are not used in Toulmin and Barton's study (1964). Since the authors of this study clearly demonstrated the consistency of their own and literature data on pyrite, the auxiliary data given by Eqs. (7), (14), and (15) can be considered at the same level of accuracy and appropriate for correct comparison of our results and Toulmin and Barton (1964) data. The FeS activity in pyrrhotite is a convenient and sensitive parameter for such comparisons.

The calculated temperature dependence of a_{FeS}^{po} in comparison with Toulmin and Barton's (1964) data from Table 2 is shown in Fig. 4. In this figure, Trend #1 shows the activity points from Toulmin and Barton (1964), Trend #2 shows the activities calculated by Eq. (16) directly from Toulmin and Barton's (1964) data in Table 2. The data sources for calculating other trends (points) are given in Table 3.

The calculation of FeS activity in pyrrhotite by Eq. (16) employs the literature data from Eq. (14), taking into account the γ–β transition. The values of $\log aS_2$ (ref) are determined from Eq. (15), and $\log aS_2$ are determined from Eq. (8) and the data from Table 1. After the least-squares treatment of the results, the temperature

Table 3
Scheme of using different initial data for calculation of the temperature dependence of the FeS activity in pyrrhotite

$\log a(S_2)$	$\Delta_f G_m(FeS_2, cr)$	
	Toulmin and Barton (1964)	Eq. (15)
Toulmin and Barton (1964)	#2	#3 (#7)
Present study	#4	#5 (#7)

(Trends #2, #3, #4, #5 and, #7 are shown in Fig. 4.)

dependence of the FeS activity in γ and β pyrrhotites in equilibrium with pyrite was defined as follows:

$$a_{FeS}^{po}(\gamma+\beta) = (0.528 \pm 9.23 \times 10^{-3}) + (2.489 \times 10^{-7} \pm 1.485 \times 10^{-5}) \cdot T(518 < T/K < 713) \quad (17)$$

According to Eq. (17), the FeS activity in pyrrhotite is almost constant over the studied temperature range and is equal to (0.528 ± 0.005). Trend #6 in Fig. 4 was plotted without accounting for the γ–β transition to illustrate the effect of this transition on the calculated a_{FeS}^{po} values.

5. Discussion

5.1. Approach to equilibrium

The equlibrium in the Cell (A) was attained quickly and reproducibly over the whole temperature range studied. This fact can be partially explained by the presence of silver sulfide in the system. $Ag_{2\pm\delta}S$ is an ion conductor and also shows some semiconductor properties (Miyatani, 1968). The relatively high mobility of silver ions and electronic conductivity resulted in the establishment of local equilibrium between the phases of the sample system, i.e., at the three-phase contact po + py + Ag_2S. The role of Ag_2S in the fast equilibration in the system Ag–Fe–S is also illustrated by the comparison of the annealing times of the systems Fe–S (Toulmin and Barton, 1964) and Ag–Fe–S (Taylor, 1970). The local equilibrium was probably reached even faster at the contact of the sample system with the solid electrolyte due to the abundance of silver ions on the electrolyte surface. It is not known if another super-ionic, Ag_3SI, forms at the interface of the working electrode and AgI and how it can influence the equilibration kinetics. However, the importance of such possibility should not be underestimated. The analysis of all the EMF measurements indicated that pyrite–pyrrhotite equilibrium in the cell was established faster at lower (550–650 K) than at higher temperatures (650–800 K).

In the symmetric Cell (B) containing the most contrast pyrrhotite compositions in the left and the right half-cells, the equilibrium ($E \approx 0$) was attained within 12–48 h over the whole temperature range studied, which was a significantly shorter time than the annealing time reported in the study by Taylor (1970). Taking into

account the near-zero possibility of gaseous sulfur exchange between the half-cells, the results confirm that the equilibrium in the system was reached through a solid-state process.

The equilibrium among pyrrhotite, pyrite, and the gas phase (in the Fe–S system) and the equilibrium between gaseous sulfur and the sulfide electrode is attained in a longer period of time, like in a cell with separate gas space (87 days at 597 K) (Schneeberg, 1973).

Special experiments were carried out to study the equilibration processes. The compositions of the samples identical to those used in EMF cells (containing the mixture of pyrite + pyrrhotite and acanthite (α-Ag_2S) and the mixture of stoichiometric troilite, pyrite, and acanthite) were characterized by X-ray powder diffraction (XRD). The XRD analysis was conducted immediately after mixing the phases or after annealing of the pressed samples in evacuated quartz capsules at 543 ± 5 K for 10 days. The pyrrhotite composition was determined by position of the $d_{(102)}$ peak, according to Toulmin and Barton (1964). It should be noted that (200), (023) and (103) peaks of acanthite (JCPDS card 14-0072) were interfering with pyrrhotite composition analysis. The X-ray patterns showed that the stoichiometric troilite was only present in the non-annealed mixture troilite + pyrite + acanthite. It was also found that the pyrrhotite composition in the annealed sample ('FeS'/$FeS_2 + Ag_2S$) differs from that in non-annealed samples, because of the different temperature of synthesis of the pyrite–pyrrhotite pair. The pyrrhotite compositions in both annealed samples were the same. These analyses made in parallel with electrochemical measurements confirmed the possibility of fast equilibration of the pyrrhotite composition with pyrite (thermodynamic equilibrium) at low temperatures in the presence of Ag_2S. If Ag_2S was absent, the equilibrium between pyrrhotite and pyrite at the same temperatures was attained within at least one order of magnitude longer times.

In addition to the results given in Table 1, three more experiments were performed with different starting pyrrhotite compositions, and all of them demonstrated an excellent reproducibility over the studied temperature range. The starting composition $Ag_2S + Ag + FeS_2$ was measured over 10 weeks, and more than 80 *E–T* data points obtained in this run showed an ideal coincidence with the Trends γ + py and β + py (see Appendix).

5.2. Precision of a_{S2} determination

The results obtained in this study confirm the necessity of revision of many widely used sets of data, which are not sufficiently accurate for the present state of the art and in the past may have caused significant errors in calculations and predictions. First of all, this concerns the electrum tarnishing method developed by Barton and Toulmin (1964) does not meet the present-day requirements for the accuracy of experimentally obtained thermodynamic data, especially in the low-temperature region. This fact was confirmed by studies of thermodynamic properties of phases in the Ag–Au–S system (Barton, 1980; Osadchii and Rappo, 2004). Despite a very good agreement of our a_{S2} data on the γ + py solvus with the smoothed data of Barton and Toulmin (1964) in the range 598–716 K, the precision of a single data point differs by at least an order of 10 in these two studies.

It was the low precision of the method that resulted in the erroneous determination of the a^{po}_{FeS} on the pyrrhotite–pyrite solvus (Toulmin and Barton, 1964). The quantitative discrepancies in the data are relatively modest, however the extrapolation (prediction) errors were substantial despite the well-grounded theoretical approach and perfectly built methodology.

Nevertheless, our temperature dependence of a_{S2}(g) on the pyrrhotite–pyrite solvus (Fig. 3, Table 2) is in a very good agreement with Toulmin and Barton's (1964) data in the overlapping temperature interval, and there is no concern with respect to the reliability of the high-temperature points. Thus, it is reasonable to describe the γ + py solvus in the whole temperature range using a single equation:

$$\log aS_2(\gamma + \text{py}) = 15.64 - 15455 \cdot T^{-1} + \exp(10.2 - 11280 \cdot T^{-1}) \quad (18)$$

Eq. (18) represents a high-temperature extension for Eq. (12) and is recommended by the authors and P. Barton (personal communication, 2006) for further use. The results of the calculations by Eq. (18) are given in Table 2 and plotted in Fig. 4.

Such good agreement can be explained by the use of the same experimental approach and the same method of aS_2 calculation. Both the electrum tarnishing method and Cell (A) sense the chemical potential of silver, which depends on the chemical potential of sulfur in the system at a constant temperature. Both processes are unaffected by the physical state of sulfur. The electrum tarnishing method is based on the equilibrium co-existence of silver sulfide and an electrum alloy with a known composition (fixed chemical potential of silver) within a narrow temperature range. Using Eq. (8), one needs to know precisely the temperature dependence of the free energy of formation of Ag_2S from silver and ideal diatomic sulfur gas (S_2, g) at 1 bar, which is taken as a standard state. The choice of the standard state is arbitrary, and S_2(g) is chosen since it is a dominating form at elevated temperatures. Thus, the transition from the electrum tarnish and EMF data to $\log a_{S2}$ is a formal procedure.

The operation principle of the gas sensor (Sato, 1971; Schneeberg, 1973; Lusk and Bray, 2002) is based on the measurement of the potential of silver on the *silver sulfide electrode* with respect to pure silver. However, the electrochemical gas sensor always yields higher $\log a_{S2(g)}$ values for the pyrrhotite–pyrite equilibrium, especially at low temperatures, reflecting the lower potential of silver, and

therefore high potential of sulfur, on the sulfide electrode. Thus, under similar conditions, the EMF of the gas sensor (E) is always higher than the EMF of Cell (A), and this difference gradually increases with decreasing temperature. As a result, the equilibrium temperature for the four-phase assemblage (silver + argentite + pyrite + pyrrhotite, $E = 0$) calculated from Lusk and Bray's data (2002) is 20–25 K lower than the temperature determined for this assemblage in our study and also in the work by Taylor (1970).

The higher potential of the gas sensor is probably due to the reaction of the gaseous sulfur with the sulfide electrode and nonstoichiometry of the silver sulfide compound described by Wagner (1953). For example, the very low mobility of sulfur compared to silver ions and possible chemisorption of sulfur on silver sulfide (Wagner, 1953) results in an increase of the EMF of the gas sensor. However, all these factors have almost no effect on the free energy of formation of Ag_2S and therefore do not undermine the accuracy of the electrum tarnishing method and our results.

5.3. FeS activity in pyrrhotite

According to the results of this study (Fig. 4), the FeS activity in pyrrhotite remains constant with decreasing temperature; while the data of Toulmin and Barton (1964) indicate a significant increase. Trends #2 and #3 (Table 3, Fig. 4) are opposite and reflect different free energies of formation of pyrite in the "rigid" points in Table 2 (Toulmin and Barton, 1964) and in the linear Eq. (15). Linear approximation of the data points for pyrite leads to the same result. Also, averaging Trends #2 and #3 yields a trend with an approximately constant activity value, $a^{po}_{FeS} \approx 0.54$. Since 0.01 units in a^{po}_{FeS} at 700 K correspond to $\sim 105\ J\ mol^{-1}$ in free energy of formation of pyrite, the observed difference does not exceed the error limits specified by Toulmin and Barton (1964). A comparison of the Trends #2 and #3 demonstrates internal inconsistencies or the effect of smoothing the original experimental and auxiliary data. We note that Toulmin and Barton obtained their a^{po}_{FeS} independently and fair enough considered this kind of internal control superfluous. However, such analysis clearly demonstrates the "rigidity" of the po + py equilibrium presented in Table 5 of Toulmin and Barton (1964). Thus, Trends #2 and #4 differ significantly and are not related. In this case, we directly compare the original experimental data on $a_{S2}(g)$ in the po + py equilibrium.

It is very important to note that by using Toulmin and Barton's (1964) data one can show that a^{po}_{FeS} is constant within an experimental error in the range from 601 to 723 K. In fact, this is the only independent confirmation of our results.

Fig. 4 also shows all experimental points from Table 1 with (Trend #5) and without (Trend #6) consideration of the phase transition; and the solid line of the Trend #5 corresponds to Eq. (17). Here, the effect of the γ–β transition is most clearly seen. The two lowest points, which show the maximum deviation from the general trend, were obtained after a long-term (several days) cell operation at 510 K (where $E(A) = 0$) and a subsequent stepwise (1 K/h) temperature increase up to readable EMF values. These points were kept in the plot to characterize the maximum deviations of EMF from zero, but they do not bear significant information and were not used in the calculation of Eq. (13).

Fig. 4, as the most convenient illustration, helps to justify a very important conclusion. The enthalpy of the β–γ transition depends on the pyrrhotite composition (Gronvold and Stolen's, 1992), reaching its maximum for the pyrrhotite composition in equilibrium with pyrite and reaching its minimum for troilite. Below the γ–β transition point, the activity and composition of pyrrhotite (Fe/S ratio) start to monotonically decrease with decreasing temperature (see Section 5.5). Then, the real position of the β + py Trend on the $a^{po}_{FeS} - T$ diagram (Fig. 4) will only depend on the enthalpy of transition in troilite (reference system) and will always lie between the limiting Trends #5 and #6, closer to Trend #6.

Trend #7 was calculated using Eq. (18). Its position below Trend #6 solely results from a different calculation order and stays within the confidence interval. In terms of FeS activity in pyrrhotite, our results confirm Barton and Skinner's (1979) assumption that at low temperatures the composition and structural properties of the pyrrhotite in equilibrium with pyrite are virtually the same as at 723–773 K, which are the temperatures determined for most natural samples. It should be also noted that the a^{po}_{FeS} estimation in this study is solely done for the purpose of comparison with Toulmin and Barton's data (1964), and the estimated values do not affect the accuracy of Trends γ + py and β + py on the $\log a_{S2}(g) - 1/T$ diagrams (Eqs. (12) and (13)).

The experimental error was estimated at $\pm 66\ J\ mol^{-1}$ in the field of β-pyrrhotite and $\pm 72\ J\ mol^{-1}$ in the field of γ-pyrrhotite. Since the calculations by Eqs. (12) and (13) do not introduce any incidental errors, the accuracy of determined $\log a_{S2}$ values is derived as ±0.018 and ±0.020, respectively. In the covered temperature range, this accuracy is almost an order of magnitude higher than the accuracy obtained by Toulmin and Barton (1964) (±0.18).

The difference is also explained by the fact that our $\log a_{S2}$ vs. $1/T$ data for the γ + py equlibrium is a linear function, while Toulmin and Barton's data (1964) from Table 2 form a nonlinear trend. This difference is important since it radically affects the position of the isopleths of FeS activity (and composition) in pyrrhotite obtained by Toulmin and Barton (1964) in both the pyrrhotite and pyrite fields.

The determination of a^{po}_{FeS} can be demonstrated using Fig. 3. The reaction producing pyrite from troilite and $S_2(g)$ or the hypothetic equilibrium troilite + pyrite is a

linear function and a reference system with $a^{tr}_{FeS} = 1$. The equilibrium po + py should be located above this reference line, since $a^{po}_{FeS} < 1$, by definition.

If experimental data form a $\log a_{S2} = f(T^{-1})$ trend that is strictly parallel to the reference system, a^{po}_{FeS} is constant in the whole temperature range and can be calculated using Eq. (16). If the lines are not parallel, a^{po}_{FeS} is a linear function of temperature, which increases in magnitude as the lines approach one another. If the po + py equilibrium is not a linear function, $a^{po}_{FeS} = f(T)$ is also nonlinear and can be determined from Eq. (16). According to Fig. 3, Toulmin and Barton's a^{po}_{FeS} decreases at temperatures above 828 K, whereas in the low-temperature region, Schneeberg's study (1973) indicates lower a^{po}_{FeS} values compared to Toulmin and Barton' data (1964) and the results of this study.

5.4. γ–β Transition in pyrrhotite

In the studied Reaction (1), the phase transition in hexagonal pyrrhotite at 601±2 K behaves as a classical transition of the first order (a disruption in the first derivative of the Gibbs energy by temperature at a constant pressure). As a result of the transition, the slope of the β-pyrrhotite + pyrite line on the diagram $\log a_{S2}$ vs. $1/T$ decreases. The temperature of the phase transition (γ–β) in hexagonal pyrrhotite (Eq. (11)) is in agreement with literature data; however, the enthalpy of the transition, (4020 ± 200) J mol^{-1}, is significantly greater than the value summarized by Kubaschewski and Evans (1958) and adopted in the Toulmin and Barton (1964) study (502 J mol^{-1}). This transition is associated with the Neel γ-paramagnetic/β-antiferromagnetic transformation (Neel, 1953) and is almost unrelated to the pyrrhotite structure and composition; the volume, however, can change (Novikov et al., 1977, 1988). Unfortunately, the method used to determine the thermal effect of the γ–β transition was not clearly specified in the literature source. If differential thermal analysis (DTA) was used for a single phase po, our enthalpy value can be considered more accurate because it was determined from equilibrium data that extensively cover the stability temperature ranges of both phases. This statement holds if the pyrrhotite composition is constant within the studied temperature range.

The enthalpy of the γ–β transition obtains a totally new meaning if the po composition on trend β + py is a function of temperature (as was discussed above). In this case, the enthalpy of transition calculated through Eq. (11) mainly reflects the compositional change in pyrrhotite on trend β + py (Eq. (10)). It is almost impossible to derive the value of the enthalpy change corresponding to the γ–β magnetic transition in pyrrhotite (as an individual phase) from our data, but these parameters can be taken into account in calculations of a^{po}_{FeS} on po + py equilibrium (Fig. 4). It should be noted that changes in γ and β pyrrhotite composition do not significantly influence the accuracy of the determined transition temperature point because the phases have the same compositions at the transition point.

From calorimetry data (Gronvold and Stolen, 1992), the γ–β transition occurs at 590 K and does not depend on the pyrrhotite composition. At the same time, the pyrrhotite composition has a strong effect on the enthalpy of transition. For the composition $Fe_{0.875}S$ (Fe_7S_8), the contribution of the γ–β transition is five times higher than that for the compositions FeS, $Fe_{0.98}S$, and $Fe_{0.89}S$. However, in the experiments with monoclinic pyrrhotite, a phase reaction producing pyrite and sulfur took place which significantly complicates data interpretation. It is not possible to determine the enthalpies of the γ–β transitions at the transition temperature of 590 K from Gronvold and Stolen's data (1992) on high-temperature heat capacities for different pyrrhotite compositions.

Vaughan and Craig (1978) reviewed a large amount of literature data on magnetic transitions in pyrrhotites, but they did not resolve any of the issues concerning the energetic of the γ–β transition. Perhaps the Neel's transition effects in hexagonal pyrrhotite in Reaction (1) and in an individual phase can differ significantly in both temperature and associated heat effect. This problem certainly needs further investigation.

5.5. Pyrrhotite compositions

As was noted above, there was no need in this study to specially determine the pyrrhotite compositions in equilibrium with pyrite. The obtained EMF data correspond to the equilibrium state between py and po at each point, as was proved by approaches to equilibrium from both sides. Thus, in some runs, troilite was used as a starting component, and in other runs, pyrrhotite was formed in situ in the EMF cell as a result of the reaction of metallic silver with pyrite (see Appendix). All the experimental trends $E = f(T)$ were identical, and equilibrium was reached within 48 h. To extrapolate the pyrrhotite compositions determined by Toulmin and Barton (1964) and confirmed by Taylor (1970) to 500 K, one needs to take into account respective changes in activity coefficients. For the correlation of our data on FeS activity in pyrrhotite with pyrrhotite compositions from Toulmin and Barton (1964), any convenient notation for pyrrhotite composition can be used (Table 2).

Nevertheless, determining the β-po compositions in equilibrium with pyrite certainly is an important task. All our samples of troilite, pyrrhotite, and po + py mixtures synthesized at temperatures above 700 K are very close in composition to the pyrrhotites of Toulmin and Barton (1964) according to the X-ray diffraction analysis. One of the points for the γ + py solvus at 673 K ($1 - x = 0.8885$) is shown in Fig. 5. Some points on the β + py solvus ($Fe_{1-x}S$ with $1 - x$ equal to 0.8956 at 595 K, 0.8956 and 0.8980 at 576 K, 0.8921 at 548 K, 0.8885 at 533 K, 0.8956 and 0.8932 at 518 K, and 0.8862 at 503 K) were obtained by annealing of

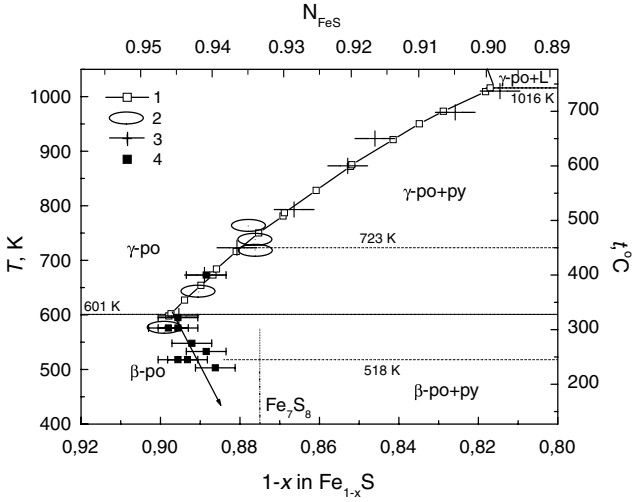

Fig. 5. Temperature-composition diagram for the pyrite–pyrrhotite solvus. 1—Rigid points of Toulmin and Barton (1964). The symbol size is not related to errors. 2—Experimental data (Table 2, Toulmin and Barton, 1964). 3—Experimental data (Arnold, 1962; as cited in Table 2 in Toulmin and Barton, 1964). 4—Present study. Horizontal bars indicate errors in composition determination ($\Delta x = \pm 0.005$). The symbol size for data of Toulmin and Barton (1964) and Arnold (1962) indicates the experimental uncertainty. $(1-x) = N_{FeS}/(2 - N_{FeS})$. The dashed lines mark the temperature range studied for Reaction (1). At temperatures below 518 K and total pressure of 1 atm, metallic silver forms at the right electrode of Cell (A) ($E = 0$). At temperatures above 723 K, the electronic conductivity of the AgI solid electrolyte may become significant.

(po + py) + Ag_2S and (tr + py + Ag_2S) mixtures, identical to the sample system in Cell (A), for two month, as described in Sections 3.1 and 3.2. Thus, the approach to equilibrium from both sides was provided.

These data demonstrate an inverse temperature dependence of the β-po pyrrhotite on the β + py solvus, opposite to that of the γ + py solvus. At the present time there are no data indicating any structural difference between γ-po and β-po. Thus, the well-known analytical relationship between the angular position of reflex (1 0 2) and the γ-po composition can be used in the β-po stability field as well. Our data on $\log a_{S2}$ vs. $1/T$ and a^{po}_{FeS} vs. T (Figs. 3 and 4) for γ and β pyrrhotites confirm that the aforesaid analytical relationship reflects the actual β pyrrhotite compositions.

The compositional extremum has a very important and obvious geological significance. In all the mineral assemblages that include hexagonal pyrrhotite and pyrite and have reached equilibrium at any temperature below 601 K, the same pyrrhotite composition will correspond to two different temperatures (Fig. 5). However, the minimal temperature principle is acceptable for natural parageneses; and in many cases, the pyrrhotite geothermometer can still be very useful.

At present, the experimental information is not sufficient to precisely locate the β + py solvus in T–x coordinates. Only the compositional extremum (at $T = 601 \pm 2$ K) is well determined.

5.6. Possibilities for data extrapolation

Eq. (13) can be formally extrapolated towards lower temperatures (taking into account the above-described assumptions), down to the point of the α-transition in pyrrhotite (410 K). According to the Fe–S phase diagram (Binary Alloy Phase Diagrams, 1987), there are no phase transformations in pyrite or hexagonal pyrrhotite above that temperature.

In the γ-pyrrhotite field, an extrapolation to higher temperatures (up to 828 K (Fig. 3), where our and Toulmin and Barton's (1964) data are in good agreement) is possible via Eq. (12). Eq. (18) is convenient to use in the whole temperature range, where the γ-pyrrhotite–pyrite solvus is stable (601–1016 K).

6. Conclusion

Studies of the phase relations in the system Ag–Fe–S by the all-solid-state galvanic cell technique produced new thermodynamic data at temperatures between 518 and 723 K and standard pressure. The obtained results are fully applicable to the system Fe–S.

The geologically significant results of this study are the following: (i) the equilibrium pyrrhotite + pyrite was extended to lower temperatures down to 518 K; (ii) the FeS activity in hexagonal γ-pyrrhotite (γ + py solvus) was found to be almost constant, $a^{po}_{FeS}(\gamma) = 0.528 \pm 0.005$, at temperatures from 723 to 601 ±2 K and at the total pressure of 1 atm; and (iii) at temperatures below 601 ±2 K, $a^{po}_{FeS}(\beta)$ and concentration of iron in β-pyrrhotite (β + py solvuse) decreases with decreasing temperature.

The above-listed conclusions are very useful for understanding some geologically important systems, such as Fe–S and Fe–Zn–S. For instance, the data for the Fe–S system confirm Barton and Skinner's (1979) assumption that at low temperatures the composition and structural properties of pyrrhotites equilibrated with pyrite are very similar to those at 723–773 K, i.e., the temperatures determined for most natural samples.

In the Zn–Fe–S system, the sphalerite composition in equilibrium with γ-pyrrhotite pyrrhotite and pyrite should be constant at temperatures below 823 K. This conclusion provides an explanation for the vertical position of the sphalerite solvus between 773 and 573 K at 1 atm, which was first determined by Boorman (1967) and later confirmed by Scott and Barnes (1971). At temperatures below the γ–β transition, Barton and Toulmin's (1966) interpretation, which states that the FeS content in sphalerite decreases with decreasing temperature, seems more credible.

It is possible to use the pyrite + hexagonal pyrrhotite equilibrium as a geological indicator of a minimal temperature.

Some additional information obtained for the Ag–Fe–S system (e.g., reaction kinetics) is of value for experimental studies. The present EMF measurements

quantitatively confirm the results of Taylor (1970), which indicated favorable conditions for equilibration in the Ag–Fe–S system. The presence of silver sulfide in the sample system (electrode) of the galvanic cell (and perhaps AgI as a solid electrolyte) accelerates the equilibration and therefore significantly extends the working temperature range. The catalytical properties of silver sulfide can be used in EMF studies of other geologically important sulfide systems, provided Ag_2S does not form additional phases or solid solutions. Candidates for such future studies include equilibria in the Co–S system.

The obvious advantages of the EMF method are high precision, relative simplicity of experimental design, and the possibility to control the data quality (equilibrium) during the experiment.

It should be rightfully noted that, in spite of the obvious benefits of the EMF method, this study as it is presented here, would not be possible without the detailed comparison of the electrochemical data with the excellent results of Toulmin and Barton (1964) and Taylor (1970) obtained via solid-state annealing techniques.

Acknowledgments

The authors thank Dr. Mark Fedkin (The Pennsylvania State University) for his participation in the experimental studies at the Laboratory of High-Temperature Electrochemistry (IEM RAS), useful discussions, and translation of this manuscript into English, and Dr. Andrey Kalinichev (University of Illinois) for valuable discussions and suggestions. We are grateful to Dr. Ninell Lichkova (Institute of Microelectronics Technology and High Purity Materials, RAS) for synthesis of an excellent solid electrolyte.

The authors are especially grateful to Dr. Paul B. Barton for very fruitful and friendly discussion, which helped us to substantially improve this manuscript although we continue to differ on some points.

Financial support was provided via Russian Foundation for Basic Research, Grants Nos. 03-05-64380 and 05-05-64237.

Associate editor: Edward M. Ripley

Appendix

To study the kinetics of equilibration and to evaluate the data reproducibility, the method of double-sided approach to equilibrium was used. Reaction (1) was studied in electrochemical cells with a priori non-equilibrium starting composition of the sample system. For instance, Cell (C) contained pyrite, silver, and acanthite as starting components:

$$(-)\mathrm{Pt}|\mathrm{Ag}|\mathrm{AgI}|\mathrm{Ag},\mathrm{Ag_2S},\mathrm{FeS_2}|\mathrm{Pt}(+) \qquad (\mathrm{C})$$

The sample system in Cell (C) is in equilibrium at temperatures below 518 K, and its composition was chosen in such a way that after complete reaction at a temperature above 518 K, the ratios of the products (po:py:Ag_2S) are equimolar.

The starting components of the sample system of Cell (D) were pyrite, troilite, and acanthite, like in one of the half-cells in symmetrical Cell (B):

$$(-)\mathrm{Pt}|\mathrm{Ag}|\mathrm{AgI}|\mathrm{tr},\mathrm{FeS_2},\mathrm{Ag_2S}|\mathrm{Pt}(+) \qquad (\mathrm{D})$$

The evaluation criterion for the equilibrium assemblage formation and the overall electrochemical process was the identity of the data obtained in these cells at each temperature to the data from Cell (A).

The results of electrochemical measurements in Cells (C) and (D) are listed in Table A1 and presented as linear equations ($\Delta_r C_p = 0$) for the fields of stability of the high-temperature (γ) pyrrhotite with pyrite and the low-temperature (β) pyrrhotite with pyrite.

$$E(\mathrm{C})\gamma + \mathrm{py},\quad \mathrm{mV} = -(310.0 \pm 1.3) + (0.5943 \pm 0.0020)\cdot T,\quad (605 < T/\mathrm{K} < 722),\quad R^2 = 0.9998 \qquad (\mathrm{A.1})$$

$$E(\mathrm{C})\beta + \mathrm{py},\quad \mathrm{mV} = -(292.8 \pm 3.8) + (0.5659 \pm 0.0067)\cdot T,\quad (522 < T/\mathrm{K} < 605),\quad R^2 = 0.9997 \qquad (\mathrm{A.2})$$

$$E(\mathrm{D})\gamma + \mathrm{py},\quad \mathrm{mV} = -(309.8 \pm 4.0) + (0.5941 \pm 0.0061)\cdot T,\quad (605 < T/\mathrm{K} < 719),\quad R^2 = 0.9998 \qquad (\mathrm{A.3})$$

$$E(\mathrm{D})\beta + \mathrm{py},\quad \mathrm{mV} = -(291.6 \pm 4.6) + (0.5639 \pm 0.0083)\cdot T,\quad (534 < T/\mathrm{K} < 605),\quad R^2 = 0.9997 \qquad (\mathrm{A.4})$$

The experimental errors were determined by the least-squares treatment for the 2σ confidence interval.

Fig. A1 shows the deviations of all experimental points obtained in Cells (A), (C), and (D) from the the linear approximations determined by the least-squares treatment for the Cell (A) data in the γ + py и β + py ranges (Eqs. (9) and (10), respectively). The doubled square root of the mean squared deviation of the experimental data of Cell (A) from the γ + py и β + py trends is also shown in Fig. A1. The 2σ values estimated for the differences between the experimental data of Cells (C) and (D) and between Eqs. (9) and (10) are 2σ (C)γ + py = 0.54, 2σ (C)β + py = 1.01, 2σ (D)γ + py = 1.04, 2σ (D)β + py = 0.99, respectively.

Another sensitive criterion for the evaluation of equilibrium and reproducibility is the coincidence of the temperatures and enthalpies of the γ–β transition in pyrrhotite. The temperature and enthalpy values calculated from Eqs. (A1)–(A4) for the phase transitions in Cells (C) and (D) are as follows:

Table A1
Measured temperature and EMF (E_{meas}) of galvanic Cells (C) and (D) and deviations of the experimental points from the values calculated via Eqs. (9) and (10) ($\Delta E = E_{meas} - E_{calc}$)

T (K)	E_{meas} (mV)	ΔE (mV)
Cell (*C*)		
522.1	3.06	0.47
527.0	5.67	0.30
529.0	6.26	−0.18
532.2	8.93	0.68
534.0	9.22	−0.05
536.2	10.50	−0.02
539.0	12.07	−0.03
541.0	13.40	0.17
544.2	14.86	−0.13
546.1	16.19	0.12
547.3	17.73	0.98
549.4	17.74	−0.19
551.3	19.21	0.20
552.5	19.35	−0.34
556.5	22.11	0.21
557.6	23.54	1.02
561.6	25.12	0.34
563.7	25.53	−0.44
566.6	27.95	0.34
567.9	27.91	−0.44
567.9	29.39	1.04
572.0	30.95	0.34
575.1	31.98	−0.39
577.0	33.81	0.36
578.2	34.89	0.77
582.0	36.72	0.44
583.3	36.78	−0.23
587.1	39.6	0.49
588.5	40.72	0.82
591.1	42.02	0.65
591.4	41.42	−0.12
594.4	43.19	−0.05
597.1	45.47	0.70
598.3	46.20	0.75
601.9	48.4	0.91
603.5	48.38	−0.07
605.5	49.59	−0.06
607.0	51.11	0.56
608.5	51.92	0.47
612.1	54.08	0.46
615.3	55.3	−0.18
617.0	57.01	0.51
618.4	57.66	0.32
621.8	59.83	0.44
625.0	61.16	−0.15
628.0	63.35	0.30
631.3	65.38	0.34
632.7	65.78	−0.10
632.7	65.75	−0.13
634.7	66.98	−0.10
637.6	69.10	0.28
641.2	71.27	0.34
644.5	72.70	−0.21
647.6	74.93	0.16
649.5	75.71	−0.21
651.4	77.28	0.22
654.7	78.88	−0.16
657.6	80.85	0.13
659.7	81.94	−0.05
661.4	83.17	0.16
664.7	84.49	−0.50
667.7	86.90	0.10
670.0	87.98	−0.14
671.8	89.41	0.21
674.9	90.82	−0.24
677.7	92.78	0.03
679.8	93.87	−0.14
681.8	95.42	0.21
684.7	96.83	−0.06
684.9	96.94	−0.07
687.5	98.69	0.11
689.7	99.77	−0.13
691.6	101.12	0.08
694.7	102.87	−0.03
697.4	104.55	0.08
699.6	105.74	−0.05
701.8	107.32	0.21
704.6	108.75	−0.04
707.2	110.42	0.06
709.5	111.69	−0.05
711.8	113.21	0.15
716.8	116.22	0.15
721.6	119.14	0.19
Cell (*D*)		
534.4	9.32	−0.18
537.0	10.84	−0.12
537.3	11.02	−0.11
537.3	11.48	0.35
540.3	13.61	0.79
542.3	14.71	0.77
546.4	16.32	0.07
548.9	18.40	0.75
554.3	21.22	0.53
563.5	26.75	0.89
557.4	22.53	0.10
562.0	25.61	0.59
570.1	29.86	0.29
578.9	34.81	0.29
584.4	38.21	0.60
589.4	40.27	−0.15
594.5	43.94	0.66
599.5	46.29	0.2
604.7	50.12	0.95
604.9	49.86	0.57
606.2	50.88	0.81
614.8	56.00	0.80
622.2	59.56	−0.06
625.2	61.53	0.12
632.3	65.01	−0.64
639.1	69.1	−0.60
645.4	73.45	−0.01
651.4	76.56	−0.48
653.8	79.00	0.52
660.0	81.42	−0.76
665.0	85.10	−0.06
671.3	88.71	−0.21
677.9	93.54	0.68
684.0	96.12	−0.38
687.9	99.21	0.38
691.3	100.90	0.04
697.2	104.25	−0.13
701.1	106.20	−0.51
707.0	110.43	0.20
713.5	114.87	0.76
719.2	117.79	0.28

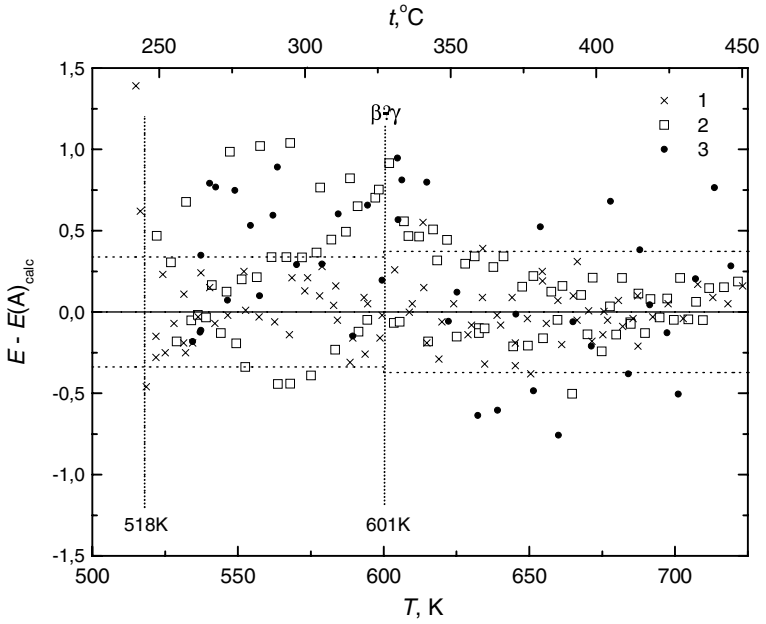

Fig. A1. Error diagram showing the consistency between Eqs. (9) and (10) and experimental data: 1—Cell (A), dashed lines indicate the confidence interval 2σ; 2—Cell (C); 3—Cell (D). Explanations are given in the text.

$$T_{\mathrm{trs}}(\mathrm{C}) = 605.6\mathrm{K}, \quad \Delta_{\mathrm{trs}}H = 3319\mathrm{J\,mol^{-1}}$$

$$T_{\mathrm{trs}}(\mathrm{D}) = 605.2\mathrm{K}, \quad \Delta_{\mathrm{trs}}H = 3527\mathrm{J\,mol^{-1}}$$

These results are self-consistent and also show a satisfactory agreement with the data of Cell (A), which indicated a slightly higher (by 4 K) transition temperature and a slightly lower (by 900–700 J $\mathrm{mol^{-1}}$) transition enthalpy.

Thus, the electrochemical studies of Reaction (1) in Cells (C) and (D) demonstrated almost complete coincidence of these data with the results from Cell (A). This fact implies that with the chosen component ratios, the sample system comes to the thermodynamic equilibrium from any starting phase composition, and the EMF values are determined by Reaction (1). Some deviations of the EMF vs. temperature trends of Cells (C) and (D) from that of Cell (A) can be explained by instrumental errors and less favorable kinetics early in the experiment at relatively low temperatures.

References

Arnold, R.G., 1962. Equilibrium relations between pyrrhotite and pyrite from 325° to 741°. *Econ. Geol.* **57**, 72–90.

Barker, W.W., Parks, T.C., 1986. The thermodynamic properties of pyrrhotite and pyrite: a re-evaluation. *Ceochim. Cosmochim. Acta* **50**, 2185–2194.

Barton, M.D., 1980. The Ag–Au–S system. *Econ. Geol.* **75**, 303–316.

Barton Jr., P.B., Skinner, B.J., 1967. Sulfide mineral stabilities. In: Barnes, H.L. (Ed.), *Geochemistry of Hyrothermal Ore Deposites*. John Wiley and Sons, pp. 278–403.

Barton, P.B., Skinner, B.J., 1979. Sulfide mineral stabilities. In: *Geochemistry of Hydrothermal Ore Deposits*. Holt, Rinehart and Winston, New York, pp. 236–333.

Barton, P.B., Toulmin, P., 1964. The electrum-tarnish method for the determination of the fugacity of sulfur in laboratory sulfide system. *Ceochim. Cosmochim. Acta* **28**, 619–640.

Barton, P.B., Toulmin, P., 1966. Phase relations involving sphalerite in the Fe–Zn–S system. *Econ. Geol.* **61**, 815–849.

Boorman, R.S., 1967. Subsolidus studies in the ZnS–FeS–FeS_2 system. *Econ. Geol.* **62**, 614–631.

Binary Alloy Phase Diagrams, 1987. Massalski, T. (Ed.), American Society for Metals.

Gronvold, F., Stolen, S., 1992. Thermodynamics of iron sulfides II. Heat capacity and thermodynamic properties of FeS and of $Fe_{0.875}S$ at temperatures from 298.15 K to 1000 K, of $Fe_{0.98}S$ from 298.15 to 800 K, and of $Fe_{0.89}S$ from 298.15 to about 650 K. Thermodynamic of formation. *J. Chem. Thermodyn.* **24**, 913–936.

Ivanov-Schits, A.K., Moorin, I.V., 2000. Ionics of Solid State, University of Saint-Petersburg, vol. I, pp. 220–232 (in Russian).

Kissin, S.A., Scott, S.D., 1982. Phase relations involving pyrrhotite below 350 °C. *Econ. Geol.* **77**, 1739–1754.

Kiukkola, K., Wagner, C., 1957a. Galvanic cells for the determination of the standard molar free energy of formation of metal halides, oxides, and sulfides at elevated temperatures. *J. Electrochem. Soc.* **104**, 308–316.

Kiukkola, K., Wagner, C., 1957b. Measurements on galvanic cells involving solid electrolytes. *J. Electrochem. Soc.* **104**, 379–386.

Kubaschewski, O., Evans, E., 1958. *Metallurgical Thermochemistry*. Pergamon Press, New York, p. 426.

Kullerud, G., Yoder Jr., H.S., 1959. Pyrite stability relations in the Fe–S system. *Econ. Geol.* **54**, 533–572.

Lusk, J., Bray, D.M., 2002. Phase relations and the electrochemical determination of sulfur fugacity for selected reactions in the Cu–Fe–S and Fe–S systems at 1 bar and temperatures between 185 and 460 °C. *Chem. Geol.* **192**, 227–248.

Lusk, J., Scott, S.D., Ford, C.E., 1993. Phase relations in the Fe–Zn–S system to 5 kbars and temperature between 325° and 150 °C. *Econ. Geol.* **88**, 1880–1903.

Miyatani, S., 1968. α-Ag_2S as a mixed conductor. *J. Phys. Soc. Jpn.* **24**, 328–336.

Neel, L., 1953. Some new results on antiferromagnetism and ferromagnetism. *Rev. Modern Phys.* **25**, 58–63.

Novikov, G.V., Egorov, V.K., Popov, V.I., Polovov, V.M., 1977. To the problem of magnetic transformation in pyrrhotites. In: Proceedings of the International Conference on Mossbauer Spectroscopy, Bucharest, pp. 371–372.

Novikov, G.V., Egorov, V.K., Sokolov, Yu.A., 1988. *Pyrrhotites: (Crystal and Magnetic Structure, Phase Transformations)*. Nauka, Moscow, 184 p.

Osadchii, E., Lunin, S., 1994. Determination of activity –composition relations in (Fe_x Zn_{1-x})S solid solutions at 859–1020 K by solid state EMF measurements. *Exp. Geosci.* **3** (2), 48–50.

Osadchii, E.G., Rappo, O.A., 2004. Determination of standard thermodynamic properties of sulfides in the Ag–Au–S system by means of solid-state galvanic cell. *Am. Mineral.* **89**, 1405–1410.

Osadchii, E., Rosen, E., Saitton, B., 1990. Equilibrium studies of the system Ni–S–O using the solid electrolyte galvanic cell technique. *Acta Chem. Scand.* **44**, 476–480.

Osadchii, E., Bostrom, D., Lunin, S., Rosen, E., 1998. Thermodynamic properties of dyscrasite (Ag_3Sb) at isostatic pressure 4000–8000 bar. *Phys. Chem. Minerals* **25**, 288–291.

Osadchii, E.G., Fed'kin, M.V., Kotova, A.A., 2002. Investigation of pyrrhotite–magnetite equilibrium by use EMF method with Ag/Ag_2S gas buffer. *Petrologiya* **10** (6), 645–655 (in Russian).

Pajryd, L., 1985. Experimental study of phase equilibria and thermodynamic stabilites in the system i-Mo–TiO_2-O at high temperatures, Thesis, University of Umea, Sweden, ISBN 91-7174-193-3.

Richardson, F.D., Jeffes, J.H.E., 1952. The thermodynamics of substances of interest in iron and steel making. *J. Iron Steel Inst.*, 165–175.

Robie, R.A., Hemingway, B.S., 1995. Thermodynamic properties of minerals and related substances at 298.15 K and 1 Bar (10^5 Pascals) pressure and at high temperatures. *US Geol. Surv. Bull.*, 2131.

Sato, M., 1971. Electrochemical measurements and control of oxygen fugacity and other gaseous fugacities with solid electrolyte systems. In: Ulmer, G.C. (Ed.), *Research Techniques for High Pressure and High Temperature*. Springer, New York, pp. 43–99 (Chapter 3).

Schneeberg, E.P., 1973. Sulfur fugacity measurements with the electrochemical cell $Ag/Ag_{2+x}S/S_2$. *Econ. Geol. Bull. Soc. Econ. Geol.* **68**, 507–517.

Scott, S.D., 1976. Application of the sphalerite geobarometer to regionally metamorphosed terrains. *Am. Mineral.* **61**, 661–670.

Scott, S.D., Barnes, H.L., 1971. Sphalerite geothermometry and geobarometry. *Econ. Geol.* **66**, 653–669.

Taylor, L.A., 1970. The system Ag–Fe–S: phase equilibria and mineral assemblages. *Mineral. Deposita* **5**, 41–58.

Toulmin III, P., Barton Jr., P.B., 1964. A thermodynamic study of pyrite and pyrrhotite. *Ceochim. Cosmochim. Acta* **28**, 641–671.

Toulmin III, P., Barton Jr., P.B., Wiggins, L.B., 1991. Commentary on the sphalerite geobarometer. *Am. Mineral.* **76**, 1038–1051.

Tretyakov, Yu.D., 1978. Solid State Reactions, M., "KHIMIYA", p. 23 (in Russian).

Vaughan, D.J., Craig, J.R., 1978. *Mineral Chemistry of Metal Sulfides*. Cambridge University Press, Cambridge.

Vaughan, D.J., Craig, J.R., 1997. Sulfide ore mineral stabilities, morphologies, and intergrowth textures. In: *Geochemistry of Hydrothermal Ore Deposits*. John Wiley & Sons, Inc., New York, pp. 367–434.

Wagner, C., 1953. Investigations on silver sulfide. *J. Chem. Phys.* **21**, 1819–1827.